

Effect of cylinder diameter and boat tail angle on the free vibration characteristics of a typical payload fairing

V. Ramamurti†

Machine Dynamics Laboratory, Indian Institute of Technology, Madras 600036, India

S. Rajarajan‡

Launch Vehicle Design Group, Vikram Sarabhai Space Centre, Trivandrum 695022, India

G. Venkateswara Rao‡†

Structural Engineering Group, Vikram Sarabhai Space Centre, Trivandrum 695022, India

Abstract. Three noded plate and shell finite element and 3D beam element in conjunction with Lanczos method are used for studying the effect of boat tail angle on the free vibration characteristics of a typical payload fairing for three different cylinder diameters with height to diameter ratio 1.5. Configurations without boat tail structural member are also studied. One half of the one side fairing structure is considered for the analysis and symmetric boundary conditions are used.

Key words: finite element method; Lanczos method; payload fairing.

1. Introduction

In launch vehicle applications, great efforts are made to understand the dynamic characteristics of different structures. Large number of experimental and theoretical studies are made to predict the dynamic behaviours of these structures before launch. These details are required to study the overall behaviour of the structural elements. Fundamental frequencies of these structures are one of the parameters required to understand the control requirements and for control system designs. These details are also required for studying the structural interactions. Eigenvalues and associated eigenvectors are required for further analysing the response behaviour of the structural elements. Payload fairing is an important structural element in any launch vehicle, protecting the spacecraft from adverse aerodynamic environments. The dynamic behaviour of this structure is to be carefully studied to ensure that the structure performs the specified functions. Different configurations are used based on the mission requirements. Many aspects of efficient payload fairing design are very well discussed by Shen and Pope (1991) and the configurations are compared based on the weight,

† Professor

‡ Scientist/Engineer

‡† Group Director

cost and payload increments. Some of the possible changes in configurations are in diameter, length, boat tail angle, forward surface, number of segments, separation system, etc. For instance the Atlas fairing is made in two halves as explained by Michael (1990) and so also the Japanese H-II rocket satellite fairing and the Indian PSLV as presented by Yasunaga *et al.* (1990) and Anjaneyalu *et al.* (1988) respectively. On the other hand, Titan 4 payload fairing is constructed in tri-sectors as explained by Stanely (1990). A complete set of data on the dynamic characteristics of a payload fairing for different parameters are required to fully understand the dynamic characteristics and also for finalising the configurations based on mission requirements. In this work, the effect of cylinder diameter and boat tail angle of a typical payload fairing on eigenvalues are presented.

2. Structural details

Typical payload fairing structure is a cone - cylinder - cone - sphere structure made in two halves. The corresponding structural members are 2 mm thick aluminium alloy boat tail with longitudinal stiffeners, aluminium isogrid cylinder with bulk head in the middle, 1.6 mm thick aluminium alloy nose cone with circumferential bulk heads and 3 mm thick steel nose cap. All the structural members have interfacing end rings apart from the edge beams with interfacing provisions and space for housing the explosive charges for imparting separation. Three different diameters viz. 3m, 4m and 5m are considered for the study with H/D ratio 1.5. The corresponding nose cap radii are 700 mm, 1176 mm and 1400 mm.

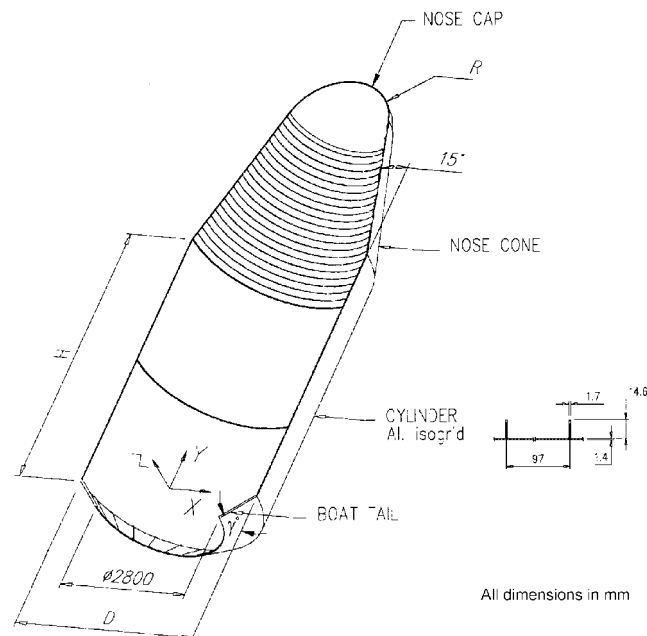


Fig. 1 Typical payload fairing configuration (one half)

Table 1 Sectional properties of beam members

Description	Area (mm ²)	Moment of inertia (mm ⁴)		
		I_{xx}	I_{yy}	I_{zz}
Nose cone forward end ring	402	61225	97380	3565
Nose cone bulk head	128	11166	33333	119
Cylinder bulk head	757	238782	128553	10390
Boat tail forward end ring	1108	371131	272033	25065
Boat tail aft end ring	1212	664364	160271	41483
Boat tail stiffeners	202	91467	30695	185
Nose cone aft end ring	895	293014	136454	12606
Nose cap ring + Nose cone forward end ring	718	201436	155217	5336
Piston beam	1362	279300	955800	6865
Nose cone edge beam	1289	469824	608174	3938
Boat tail edge beam	841	91841	374713	7959

3. Finite element formulation

3.1 Plate and shell element

Plate and shell finite elements are used for modelling the shells as an assemblage of flat plate elements. This is a 3 noded triangular element with 6 degrees of freedom per node viz., three axial displacements u , v , w and three rotations θ_x , θ_y , θ_z . Typical finite element and the nodal degrees of freedom are shown in Fig. 2. Since the in-plane and bending behaviours are uncoupled for an isotropic plate, the individual stiffness matrices are separately obtained and then combined to give the element stiffness matrix, using natural coordinates.

The in-plane strain energy P_1 and the flexural strain energy P_2 are given by

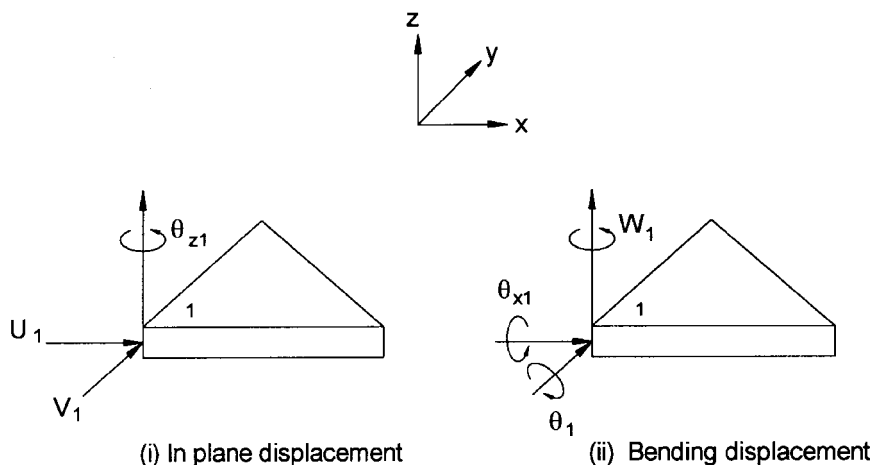


Fig. 2 Three noded plate and shell element

$$\begin{aligned}
P_1 &= \frac{1}{2} \iint_A \{\epsilon_p\}^T \{\sigma_p\} dA \\
&= \frac{1}{2} \iint_A \{\epsilon_p\}^T \{D_p\} \{\epsilon_p\} dA
\end{aligned} \tag{1}$$

$$\begin{aligned}
P_2 &= \frac{1}{2} \iint_A \{\epsilon_f\}^T \{\sigma_f\} dA \\
&= \frac{1}{2} \iint_A \{\epsilon_f\}^T \{D_f\} \{\epsilon_f\} dA
\end{aligned} \tag{2}$$

where $\{\sigma_p\}$ and $\{\sigma_f\}$ are the in-plane stress resultants and bending & twisting moments.

In-plane strain $\{\epsilon_p\}$ and bending strain $\{\epsilon_f\}$ are given by

$$\{\epsilon_p\} = \begin{Bmatrix} \epsilon_x \\ \epsilon_y \\ \gamma_{xy} \end{Bmatrix} = \begin{Bmatrix} \partial u / \partial x \\ \partial v / \partial y \\ \frac{\partial u}{\partial y} + \frac{\partial v}{\partial x} \end{Bmatrix} \tag{3}$$

$$\{\epsilon_f\} = \begin{Bmatrix} -\partial^2 w / \partial x^2 \\ -\partial^2 w / \partial y^2 \\ -2\partial^2 w / \partial x \partial y \end{Bmatrix} \tag{4}$$

A linear polynomial for the in-plane displacements and a cubic polynomial (Zienkiewicz 1971) for bending displacements in area coordinates L_1 , L_2 and L_3 are used.

$$\begin{aligned}
u &= \beta_1 L_1 + \beta_2 L_2 + \beta_3 L_3 \\
v &= \beta_4 L_1 + \beta_5 L_2 + \beta_6 L_3 \\
w &= \alpha_1 L_1 + \alpha_2 L_2 + \alpha_3 L_3 + \alpha_4 \left(L_2^2 L_1 + \frac{1}{2} L_1 L_2 L_3 \right) + \alpha_5 \left(L_1^2 L_2 + \frac{1}{2} L_1 L_2 L_3 \right) + \alpha_6 \left(L_3^2 L_2 + \frac{1}{2} L_1 L_2 L_3 \right) \\
&\quad + \alpha_7 \left(L_2^2 L_3 + \frac{1}{2} L_1 L_2 L_3 \right) + \alpha_8 \left(L_3^2 L_1 + \frac{1}{2} L_1 L_2 L_3 \right) + \alpha_9 \left(L_1^2 L_3 + \frac{1}{2} L_1 L_2 L_3 \right)
\end{aligned} \tag{5}$$

Using the above functions, the in-plane and flexural shape functions $[N_p]$ and $[N_f]$ and element stiffness matrices $[k_p]$ and $[k_f]$ are obtained by the usual procedures.

The element stiffness matrix is made up of the following submatrices

$$[k_e] = \begin{bmatrix} k_p & 0 & 0 \\ 0 & k_f & 0 \\ 0 & 0 & k_{\theta_z} \end{bmatrix} \tag{6}$$

where k_{θ_z} is an arbitrary fictitious stiffness coefficient.

The element consistent mass matrix is given by

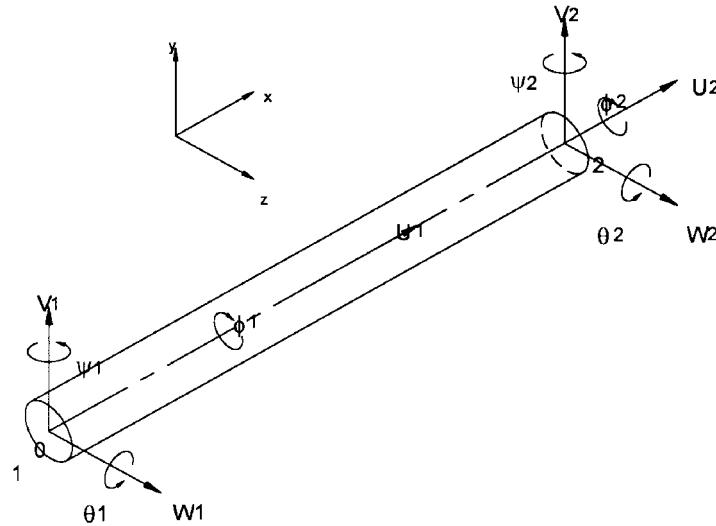


Fig. 3 Two noded 3D beam element

$$[m] = \int_{vol} \rho [N]^T [N] dv \tag{7}$$

where

$$[N] = \begin{bmatrix} [N_p] & 0 \\ 0 & [N_f] \end{bmatrix} \tag{8}$$

3.2 3D beam element

The stiffeners, end rings, edge beams, and bulk head are modelled using 2 noded beam element with 6 degrees of freedom with the displacements $u_1, v_1, w_1, \phi_1, \theta_1, u_2, v_2, w_2, \phi_2, \theta_2$ where, u is the axial displacement in x direction and v and w are lateral deflections due to bending in y and z directions as shown in Fig. 3. Linear variation has been assumed for the axial displacement and cubic polynomials for the lateral displacements (Ramamurti 2000).

4. Eigenvalue analysis

The equation of motion for a free vibration problem is given by

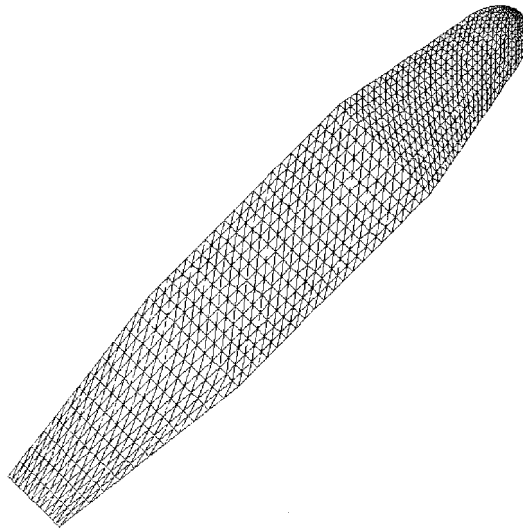
$$[M]\{\ddot{\delta}\} + [K]\{\delta\} = 0 \tag{9}$$

Lanczos' method in conjunction with inverse iteration is used for eigenvalue analysis.

Free vibration analysis is carried for the cylinder diameters 3m, 4m and 5m for different boat tail angles in steps of 10^0 from 10^0 to 80^0 . For each chosen cylinder diameter a configuration without boat tail structural element is also considered. Half model of one side of the fairing is used for the

Table 2 Finite element mesh details for boat tail angle 10^0

Configuration	No. of plate & shell elements	No. of beam elements	Total no. of nodes	Unconstrained degrees of freedom
$\phi 3\text{m}$ cylinder	1417	442	771	4458
$\phi 4\text{m}$ cylinder	1651	568	897	5187
$\phi 5\text{m}$ cylinder	1651	568	897	5187

Fig. 4 Finite element idealisation of the structure ($D=5\text{ m}$; $\gamma=10^0$)

analysis and symmetric boundary conditions are applied. The decrease in boat tail angle means increase in the height of the boat tail structural element and overall increase in the height of the payload fairing. Finite element mesh details for 10^0 boat tail angle are given in Table 2 and the idealisation for $D = 5\text{m}$; $\gamma = 10^0$ configuration is shown in Fig. 4.

5. Validation of the formulation

The formulation for eigenvalue analysis is validated using MSC NASTRAN finite element package for all the three chosen diameters with boat tail angle 30^0 and the frequencies compare very well as presented in Table 2.

6. Results and discussions

First five flexible mode frequencies for different boat tail angles for the chosen cylinder diameters are provided in Table 4-6. Increase in boat tail angle has an increasing effect on the eigenvalues. Between 10^0 and 80^0 boat tail angles the variation in the first flexible mode frequencies are to the

Table 3 Validation of eigenvalue formulation with MSC NASTRAN finite element package for boat tail angle 30°

Mode No.	Frequencies (Hz) for ϕ 3m cylinder			Frequencies (Hz) for ϕ 4m cylinder			Frequencies (Hz) for ϕ 5m cylinder		
	Present	MSC NASTRAN	Percent deviation	Present	MSC NASTRAN	Percent deviation	Present	MSC NASTRAN	Percent deviation
1	4.12	4.06	1.45	2.39	2.37	0.84	1.50	1.50	0.00
2	6.47	6.41	0.93	3.83	3.83	0.00	2.67	2.68	-0.37
3	16.66	16.58	0.48	7.97	8.25	-3.40	4.80	4.84	0.83

Table 4 Frequencies for different boat tail configurations (H/D=1.5; D=3.0m)

Mode No.	Boat tail angle								
	Without boat tail	10°	20°	30°	40°	50°	60°	70°	80°
1	2.43	3.12	3.59	4.12	4.60	4.94	5.13	5.23	5.29
2	6.08	5.74	6.11	6.47	7.08	8.09	9.45	11.09	12.45
3	13.83	15.30	16.24	16.66	16.93	17.17	17.38	17.72	18.16
4	17.86	18.50	22.12	24.91	25.57	25.90	25.94	26.05	26.22
5	26.50	24.7	25.87	28.12	32.98	36.70	37.66	38.03	38.27

Table 5 Frequencies for different boat tail configurations (H/D=1.5; D=4.0m)

Mode No.	Boat tail angle								
	Without boat tail	10°	20°	30°	40°	50°	60°	70°	80°
1	1.34	1.70	2.07	2.39	2.67	2.87	3.00	3.08	3.14
2	3.62	2.87	3.40	3.83	4.40	5.26	6.49	7.84	8.55
3	7.70	5.68	7.13	7.97	8.46	8.79	9.14	9.86	11.47
4	9.49	9.76	10.57	11.19	11.64	11.98	12.28	12.54	13.05
5	13.65	12.13	14.85	16.15	17.17	17.97	18.62	19.12	19.52

Table 6 Frequencies for different boat tail configurations (H/D=1.5; D=5.0m)

Mode No.	Boat tail angle								
	Without boat tail	10°	20°	30°	40°	50°	60°	70°	80°
1	1.19	1.08	1.32	1.50	1.67	1.78	1.86	1.92	1.96
2	2.71	1.88	2.32	2.67	3.11	3.63	4.27	4.87	5.30
3	6.38	3.13	4.05	4.80	5.41	5.83	6.21	6.57	6.81
4	7.80	5.72	6.59	6.86	7.10	7.34	7.65	8.04	8.41
5	11.01	7.08	9.18	9.69	10.05	10.31	10.55	10.76	11.04

maximum extent of 70%, 85% and 82% for 3m, 4m and 5m diameter cylinders respectively. In the case of without boat tail configurations, the boat tail aft end ring is provided in the place of boat tail forward end ring for interface requirements. The first flexible node frequencies without boat tail configurations for 3m and 4m diameters are less than the configurations with boat tail structural

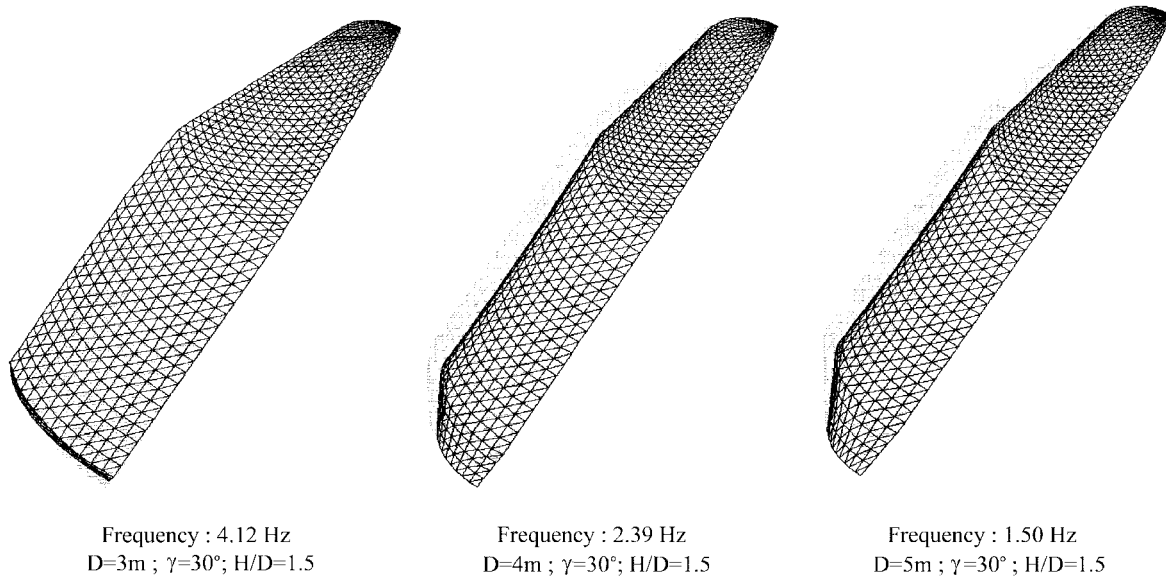


Fig. 5 First flexible mode shapes

element and slightly more than 10^0 boat tail configuration in the case of 5m diameter. The increase in cylinder diameter has a decreasing effect on the eigenvalues. The 3m diameter configuration is exhibiting highest frequencies among the cases considered for the present study. The effect of boat tail angle on the eigenvalues is felt maximum for the 4m diameter configuration. The first flexible mode shapes are given in Fig. 5 superimposed over the original geometry.

7. Conclusions

Free vibration studies are carried out using 3 noded plate and shell finite element and 3D beam element in conjunction with Lanczos method on a typical payload fairing with H/D ratio 1.5 for various boat tail angles and cylinder diameters. The formulation is validated with MSC NASTRAN finite element package. Configurations without boat tail structural member are also included in the study. The increase in cylinder diameter has a decreasing effect on the frequencies. The effect of boat tail angle is found to have maximum effect on frequencies for 4m cylinder diameter configuration. The configuration without boat tail and with small boat tail angles are generally observed to be very flexible. Huge data generated in this study are useful in further studying the structural/control system interactions, for assessing the response characteristics due to various environments encountered during the flight and for finalising the configurations for different mission requirements.

References

Anjaneyalu, M., Sudhakara Rao, K., and Srinivasan, S. (1988), "The polar satellite launch vehicle and mission

- for the Indian remote sensing spacecraft”, *Proceedings of 39th congress of the international astronomical federation*. Bangalore, India, 1-8.
- Kandebo Stanely, W. (1990), “Payload capacity of Titan 4 to expand with new fairing”, *Aviation week & Space technology*, 58-62.
- Ramamurti, V. (2000), *Computer Aided Mechanical Design and Analysis*, 4th edition, Tata McGraw-Hill publishing company, NewDelhi.
- Robbins Michael, J. (1990), “Ground test program for new Atlas payload fairing”, *Research in structures, structural dynamics and materials*, Long Beach, California, 194-205, NASA CP 3064.
- Shen, F., and Pope, D. (April 1991), “Fairing structure for space launch vehicles”, *Aerospace Engineering*, 19-22.
- Yasunaga, Y., Fukushima, Y., Nakamura, T., and Fujita, T. (1990), “Separation jettison test of Japanese H-II rocket satellite fairing”, *Proceedings of 28th Aerospace sciences meeting*, Reno, Nevada, 1-8. AIAA 90-0720.
- Zienkiewicz, O.C. (1971), *The Finite Element Method in Engineering Sciences*, 2nd edn, McGraw-Hill Publications, London.

Notation

A	area of the element
$[D_p], [D_f]$	in plane and bending stress-strain matrix
H/D	ratio of height (H) to diameter (D) of the cylinder
$[K]$	assembled global stiffness matrix
$[k_e]$	element stiffness matrix
$[k_p], [k_f]$	element in plane and bending stiffness matrix
$[k_{\theta e}]$	fictitious stiffness coefficient
L_1, L_2, L_3	area coordinates
$[M]$	assembled global mass matrix
$[m]$	element mass matrix
$[N_p], [N_f]$	in plane and bending shape functions for plate and shell element
$[N_{bm}]$	shape function for 3D beam element
P_1, P_2	in-plane and flexural strain energy
R	nose cap radius
V	volume
$\{u, v, w\}$	nodal displacements
α, β	constants
$\{\delta\}$	nodal displacement vector of the beam element
$\{\varepsilon_p\}, \{\varepsilon_f\}$	in plane and bending strain
$\{\phi, \varphi, \theta\}$	nodal rotations
γ	boat tail angle
ρ	Density
$\{\sigma_p\}, \{\sigma_f\}$	stress resultants and bending & twisting moments